Substrate-Binding Reactions of the $^3[d\sigma^*p\sigma]$ Excited State of Binuclear Gold(I) Complexes with Bridging Bis(dicyclohexylphosphino)methane Ligands: Emission and Time-Resolved Absorption Spectroscopic Studies

Wen-Fu Fu, Kwok-Chu Chan, Kung-Kai Cheung, and Chi-Ming Che*[a]

Abstract: The complexes $[Au_2(dcpm)_2]Y_2$ (dcpm = bis(dicyclohexylphosphino)methane; $Y = ClO_4^-$ (**1**), PF_6^- (**2**), $CF_3SO_3^-$ (**3**), $Au(CN)_2^-$ (**4**), Cl^- (**5**), SCN^- (**6**) and I^- (**7**)) were prepared, and the structures of **1** and **4**–**7** were determined by X-ray crystallography. Complexes **1**–**4** display intense phosphorescence with λ_{max} at 360–368 nm in the solid state at room temperature as well as in glassy solutions at 77 K. The solid-state emission quantum yields of the powdered samples are 0.37 (**1**), 0.74 (**2**), 0.53 (**3**) and 0.12 (**4**). Crystalline solid **5** displays both high-energy UV ($\lambda_{max} = 366$ nm) and low-energy visible emissions ($\lambda_{max} = 505$ nm) at room temperature, whereas either **6** or **7** shows only an intense emission with λ_{max} at 465 or 473 nm, respectively. All the complexes in degassed acetonitrile solutions exhibit an intense phosphorescence with λ_{max} ranging from 490 to 530 nm. The high-energy UV emission is assigned to the intrinsic emission of the $^3[d\sigma^*p\sigma]$ excited state of $[Au_2(dcpm)_2]^{2+}$, whereas the visible emission is attributed to the adduct formation of the triplet excited state with the solvent/counterion. The quenching rate constants of the visible emission of $[Au_2(dcpm)_2]^{2+}$ in acetonitrile by various anions are 6.08×10^5 (ClO_4^-), 9.18×10^5 (PF_6^-), 1.55×10^7 (Cl^-) and 4.06×10^9 (I^-) $mol^{-1}\,dm^3\,s^{-1}$. The triplet-state difference absorption spectra of **1**–**4** in acetonitrile show an absorption band with λ_{max} at 350 nm and a shoulder/absorption maxima at 395–420 nm; their relative intensities are dependent upon the halide ion present in solution. Substrate binding reactions of the $^3[d\sigma^*p\sigma]$ excited state with halide (X^-) to give $[Au_2(dcpm)_2X]^{+*}$ would account for the lower energy absorption maxima in the triplet-state difference absorption spectra. With iodide as the counterion, complex **7** undergoes a photoinduced electron-transfer reaction with I^- to give the radical anion I_2^-.

Keywords: binuclear complexes · exciplexes · gold · luminescence · quenching

Introduction

An important class of reactions in inorganic photochemistry is the substrate-binding reaction involving a metal ion in a electronically excited state.[1–5] These reactions are of importance with regards to molecular exciplex formation,[2, 3] which usually proceeds with coordinatively unsaturated metal complexes, such as the four-coordinate d^8[4] and two-coordinate d^{10} metal species;[2, 5] however, there only a few studies to be found in the literature. In the context of developing luminescent probes for molecular recognition and light-induced inner-sphere atom-transfer reactions,[1] these reactions are of paramount importance as they bring the excited-state molecule and its reaction partner into close proximity so that chemical reactions or sensing can occur. While molecular exciplexes have been well studied in organic photochemistry, documentary evidence for inorganic exciplex emissions is sparse in the literature.[2b, 3–6] Previous studies by McMillin and co-workers had highlighted the importance of the effect of copper(I)–solvent exciplex formation on the photophysical and photochemical properties of luminescent d^{10} copper(I) complexes.[3] Our approach to develop new photocatalysts for light-induced atom-transfer reactions is to explore the photochemistry of coordinatively unsaturated gold(I) complexes.[2b, 7] The two-coordinate d^{10} gold(I) complexes are of particular interest: this class of complexes has vacant coordination sites at the gold atom, are readily prepared and are stable towards air and moisture, but yet possess rich photoluminescence properties.[8–10] For dinuclear gold(I) complexes with two gold(I) centers held in close proximity, a lower energy $5d\sigma^* \rightarrow 6p\sigma$ transition with a red-shift in energy from its mononuclear counterpart is reported.[11] Excitation of the weakly bonded dinuclear and polynuclear gold(I) complexes into the $5d\sigma^* \rightarrow 6p\sigma$ transition would produce the $^3[d\sigma^*p\sigma]$ excited state, which has a formal metal–metal single bond and has been attributed to be responsible for their visible photoluminescence in many instances.[2b, 11] Recent preliminary work by our group, however, has suggested that the

[a] Prof. C.-M. Che, Dr. W.-F. Fu, Dr. K.-C. Chan, Dr. K.-K. Cheung
Department of Chemistry
The University of Hong Kong
Pokfulam Road, Hong Kong
Fax: (+852) 2857-1586
E-mail: cmche@hkucc.hku.hk

  0947-6539/01/0721-4656 $ 17.50+.50/0

visible emissions of the $[Au_2(dcpm)_2]Y_2$ ($Y = ClO_4^-$ (**1**), PF_6^- (**2**), $SO_3CF_3^-$ (**3**), $Au(CN)_2^-$ (**4**), Cl^- (**5**), SCN^- (**6**) and I^- (**7**); dcpm = bis(dicyclohexylphosphino)methane) systems, with intramolecular $Au^I \cdots Au^I$ separations between 2.92–3.02 Å, come from exciplexes as a result of the solvent/counterion and the $^3[d\sigma^*p\sigma]$ excited-state association.[2b] In these dinuclear gold(I) systems, dcpm was chosen as the bridging ligand, since its intraligand transitions occur at much higher energy than $5d\sigma^* \rightarrow 6p\sigma$ transitions. Here we present results from emission and time-resolved absorption spectroscopy revealing that the $^3[d\sigma^*p\sigma]$ excited state of $[Au_2(dcpm)_2]^{2+}$ readily undergoes substrate-binding reactions. The present findings highlight the important role of gold–ligand bonding in affecting the photophysical and photochemical properties of photoluminescent gold(I) complexes.

Results and Discussion

Crystal structures: The structures of the complexes **1** and **4**–**7** have been determined by X-ray diffraction, and some of the results have been communicated elsewhere.[2b] The perspective views of the molecules **1**, **4**, **5** and **7** are shown in Figures 1–4, and the crystallographic data are listed in Tables 1 and 2. Depending on the conditions of crystallisation, complex **7** could be obtained in two crystalline forms, namely, $[Au_2(dcpm)_2]I_2$ (**7a**) and $[Au_2(dcpm)_2]I_2 \cdot 0.5\,CH_2Cl_2$ (**7b**).

In all the complexes prepared in this work, the gold atom adopts a linear coordination while displaying significant $Au \cdots Au$ interactions. The crystal structures of all the gold(I) complexes reveal a T-shaped geometry at the gold atom. The Au–Au distances found in these gold(I) complexes (**1**: 2.9389(9), **4**: 2.9876(5), **5**: 2.9925(2), **6**: 2.9821(7), **7**: 3.0756(6) Å) are within the range expected for weak Au–Au interactions.[12] The gold–anion distance in $[Au_2(dcpm)_2]$-

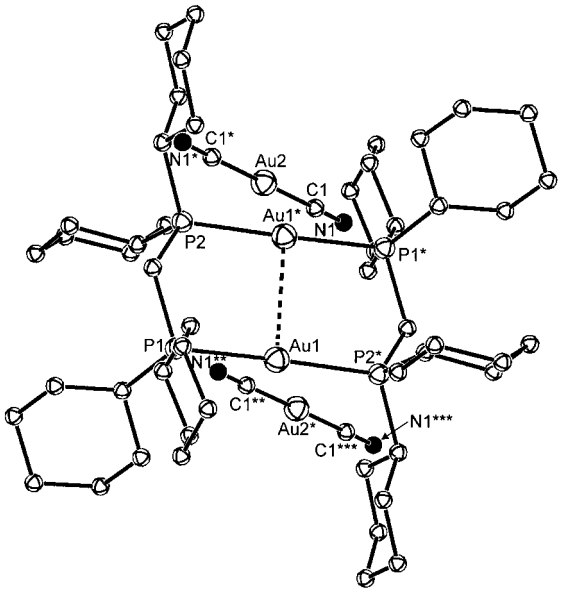

Figure 2. ORTEP drawing of $[Au_2(dcpm)_2][Au(CN)_2]_2$ (**4**).

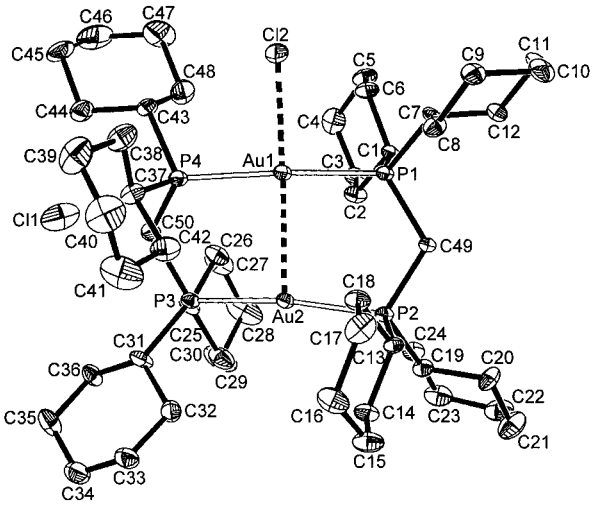

Figure 3. ORTEP drawing of $[Au_2(dcpm)_2]Cl_2$ (**5**).

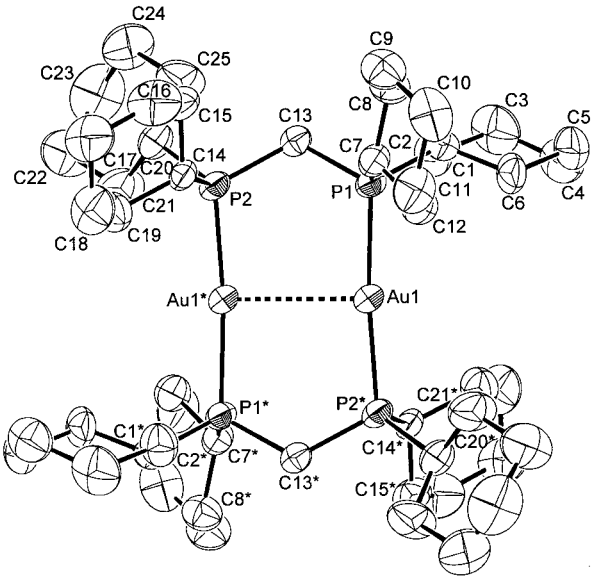

Figure 1. ORTEP drawing of $[Au_2(dcpm)_2](CO_4)_2$ (**1**) (the counter-anions are not shown). The closest Au contact with a ClO_4^- oxygen is 3.36(2) Å.

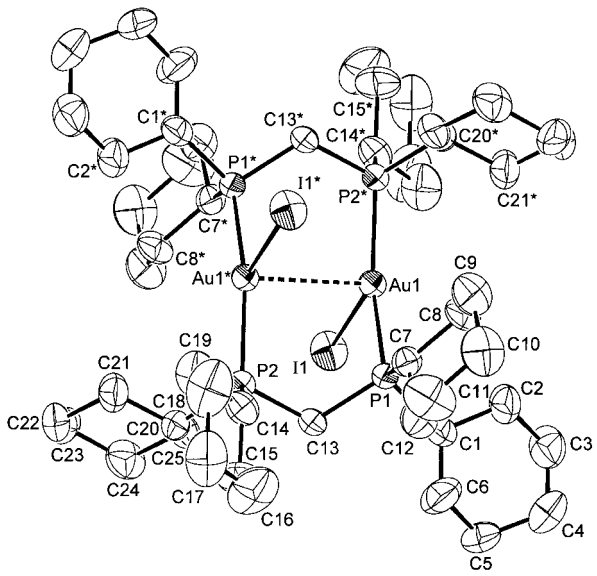

Figure 4. ORTEP drawing of $[Au_2(dcpm)_2]I_2$ (**7**).

Table 1. Selected crystallographic and data collection parameters for complexes **1** and **4**–**7**.

	1	**4**	**5**	**6**	**7a**
formula	$Au_2C_{50}H_{92}P_4 \cdot 2ClO_4$	$Au_2C_{50}H_{92}P_4 \cdot 2Au(CN)_2$	$Au_2C_{50}H_{92}P_4Cl_2 \cdot 0.25CH_3OH$	$Au_2C_{50}H_{92}P_4 \cdot 2SCN$	$Au_2C_{50}H_{92}P_4I_2$
M_r	1410.01	1709.11	1290.02	1327.28	1464.09
T [K]	301	301	293	301	301
crystal system	monoclinic	triclinic	monoclinic	tetragonal	triclinic
space group	$P2_1/a$ (No. 14)	$P\bar{1}$ (No. 2)	$P2_1/c$ (No. 14)	$I4_1/a$ (No. 88)	$P\bar{1}$ (No. 2)
a [Å]	17.812(5)	12.399(2)	19.1931(14)	30.140(3)	13.702(9)
b [Å]	14.733(4)	12.984(2)	21.6614(16)		14.712(5)
c [Å]	23.156(4)	10.904(2)	29.064(2)	12.872(2)	15.978(4)
α [°]		113.56(1)			81.18(2)
β [°]	107.98(2)	108.79(1)	94.066(2)		73.15(2)
γ [°]		95.83(1)			66.78(2)
V [Å^3]	5779.(2)	1468.7(5)	12053(2)	11693(2)	2830(2)
Z	4	1	8	8	2
ρ_{calcd} [g cm^{-1}]	1.620	1.932	1.413	1.508	1.719
$\mu(Mo_{K\alpha})$ [cm^{-1}]	53.02	101.39	50.86	52.44	64.31
crystal size [mm]	0.25 × 0.20 × 0.15	0.20 × 0.15 × 0.30	0.20 × 0.18 × 0.12	0.25 × 0.20 × 0.10	0.20 × 0.15 × 0.10
$F(000)$	2832	820	5124	5344	1432
$2\theta_{max}$ [°]	50	50	55	51	50
unique reflections	10617	5167	27694	5591	9956
parameters	555	301	1054	280	523
R_f	0.041	0.036	0.051	0.047	0.033
R_w	0.056	0.046	0.134	0.068	0.043
goodness of fit	1.64	2.03	0.814	2.59	1.20
residual electron density [e Å^{-3}]	1.09/ – 0.80	1.95/ – 2.29	1.052/ – 1.082	1.21/ – 0.94	1.04/ – 0.79

Table 2. Selected bond lengths [Å] and bond angles [°] of **1**, **4**, **5** and **7**.

Complex **1**			
Au1 ··· Au1*	2.9389(9)	Au1–P1	2.317(3)
Au1–P2*	2.320(3)	Cl1–O1	1.45(2)
Cl1–O2	1.35(2)	Cl1–O3	1.35(2)
Cl1–O4	1.48(2)		
Au1*-Au1-P1	93.31(8)	Au1-Au1*-P2	91.20(8)
P1-Au1-P2*	173.9(1)	O1-Cl1-O2	114(1)
O1-Cl1-O4	107(1)		
Complex **4**			
Au1 ··· Au1*	2.9876(5)	Au1*–P2	2.307(2)
Au1–P1	2.316(2)	Au2–C1	1.98(1)
Au2–C1*	1.97(1)	N1–C1	1.12(1)
N1*–C1*	1.15(1)	Au1* ··· N1	3.33(1)
Au1*-Au1-P1	94.25(4)	Au1-Au1*-P2	89.66(4)
P1-Au1-P2*	173.92(6)	C1-Au2-C1*	180.0
Au2-C1-N1	179(1)	Au2-C1*-N1*	178(1)
Complex **5**			
Au1 ··· Au2	2.9925(2)	Au1–P1	2.3275(8)
Au1–P4	2.3261(8)	Au2–P2	2.3086(8)
Au2–P3	2.3091(8)	Au1 ··· Cl2	2.7755(9)
Au1-Au2-P2	95.54(2)	Au1-Au2-P3	95.02(2)
Au2-Au1-P1	85.58(2)	Au2-Au1-P4	87.60 (2)
P1-Au1-Cl2	97.10(3)	P4-Au1-Cl2	91.21(3)
Cl2-Au1-Au2	171.89(2)		
Complex **7**			
Au1 ··· Au1*	3.0756(6)	Au1–I1	2.9960(7)
Au1–P1	2.342(3)	Au1–P2*	2.321(2)
Au1-Au1*-I1*	98.21(2)	Au1-Au1*-P1*	83.72(5)
Au1-Au1*-P2	94.31(5)	I1-Au1-P1	94.40(6)
I1-Au1-P2*	107.62(6)	P1-Au1-P2*	157.93(7)

$Cl_2 \cdot 0.25CH_3OH$ (**5**) differs from those in the $[Au_2(dcpm)_2](SCN)_2$ and $[Au_2(dcpm)_2]I_2$ salts, which exhibit close gold–anion contacts at both gold atoms. However, for **5**, only one of the two gold atoms has a short Au–Cl contact (2.7755(9) Å, see Figure 3), and it is the shortest Au–anion contact found in this work (cf. Au ··· I = 2.9960(7); Au ··· SCN = 3.011(3); Au ··· $Au(CN)_2$ = 3.33(1); Au ··· $OClO_3$ = 3.36(2) Å). As discussed below, the variation of the gold–anion contact has a significant effect on the solid-state emission of the gold(I) complexes studied in this work. Accordingly, complex **7** has a ^{31}P NMR chemical shift (δ = 48.5) that is lowest among the gold(I) complexes studied in this work. Indeed the ^{31}P chemical (δ) shifts of $[Au_2(dcpm)_2]Y_2$ are in the order **1**–**4** (54.1) > **5** (52.9) > **6** (50.1) > **7** (48.5), which is in agreement with the order of softness of the Y^- ions, $I^- > SCN^- > Cl^- > ClO_4^-$, PF_6^-, $CF_3SO_3^-$.

Electronic absorption spectra: Complexes **1**–**4** have similar UV/Vis absorption spectra in acetonitrile (Figure 5, solid line), and we assign the intense absorption band at 277 nm ($\varepsilon = 2.6-2.9 \times 10^4$) to the $^1(5d\sigma^* \rightarrow 6p\sigma)$ transition. The assignment is based on our recent resonance Raman studies of some dinuclear gold(I) complexes.[11] A weak shoulder at λ = 310 nm ($\varepsilon \approx 400$) is attributed to the corresponding singlet–

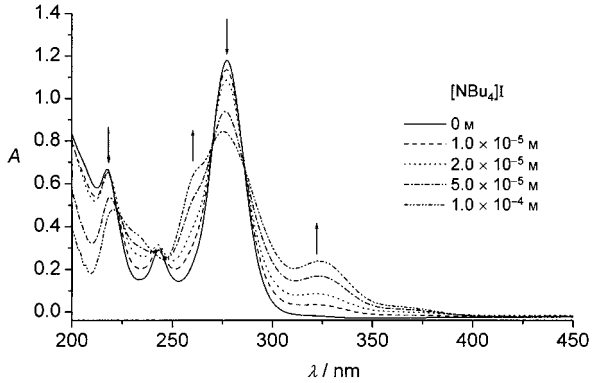

Figure 5. UV/Vis spectral changes of $[Au_2(dcpm)_2](ClO_4)_2$ (**1**) in degassed acetonitrile at room temperature as a function of the $[NBu_4]I$ concentration (with the same concentration of $[NBu_4]I$ in acetonitrile as the background).

0947-6539/01/0721-4658 $ 17.50+.50/0 *Chem. Eur. J.* **2001**, *7*, No. 21

triplet transition. Similar weak shoulders at 320 nm have been reported for $[Au_2(dmpm)_2](ClO_4)_2$ (dmpm = bis(dimethylphosphino)methane) and $[Au_2(dmpe)_2](ClO_4)_2$ (dmpe = bis(dimethylphosphino)ethane).[13]

The UV/Vis absorption spectrum of the iodide salt (i.e., **7**) differs significantly from those of the other gold(I) complexes. The intense band at $\lambda = 275$ nm, which has a similar band shape and energy to the 277 nm absorption band of the $[Au_2(dcpm)_2]^{2+}$ ion, can be reasonably assigned to the $^1(d\sigma^* \rightarrow p\sigma)$ transition. However, a definitive assignment of the absorption at 246 nm ($\varepsilon = 3.7 \times 10^4$) remains problematic because of the strong absorption of the iodide anion in a similar spectral region. While complexes **1**–**6** absorb weakly at $\lambda \geq 310$ nm, complex **7** shows intense absorptions at 323 and 365 nm with $\varepsilon = 6.1 \times 10^3$ and 1.3×10^3, respectively. These two intense absorption bands can be explained by the coordination of the I^- ion to the ground state $[Au_2(dcpm)_2]^{2+}$ complex [Eq. (1)].

$$[Au_2(dcpm)_2]^{2+} + I^- \rightleftharpoons [Au_2(dcpm)_2]I^+ \quad (1)$$

Note that the ^{31}P NMR signal of the phosphine ligand in **7** appears at higher field ($\delta = 48.5$) than those of the phosphine ligands in complexes **1**–**4** ($\delta = 54.1$), which contain non-coordinating counterions; this may be indicative of the iodide coordination to the gold atom, which would lead to less deshielded phosphorus atoms.

Figures 6 and 7 depict the UV/Vis spectral changes for "$[Au_2(dcpm)_2](SO_3CF_3)_2$ (**3**) + $[NBu_4]Br$" and "$[Au_2(dcpm)_2]Cl_2$ (**5**) + $[NBu_4]Cl$" in acetonitrile as a function of the concentration. These spectral changes are attributed to the reaction given in Equation (2).

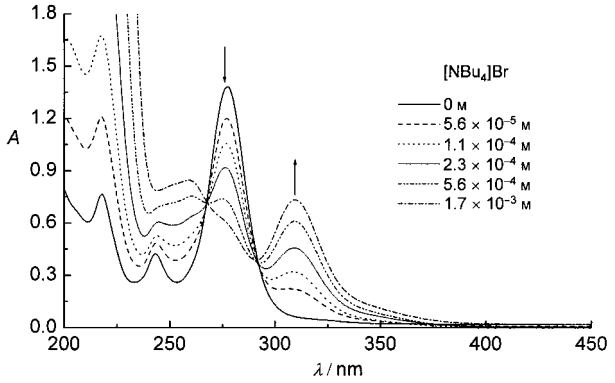

Figure 6. UV/Vis spectral changes of $[Au_2(dcpm)_2](SO_3CF_3)_2$ (**3**) in degassed acetonitrile at room temperature as a function of the $[NBu_4]Br$ concentration.

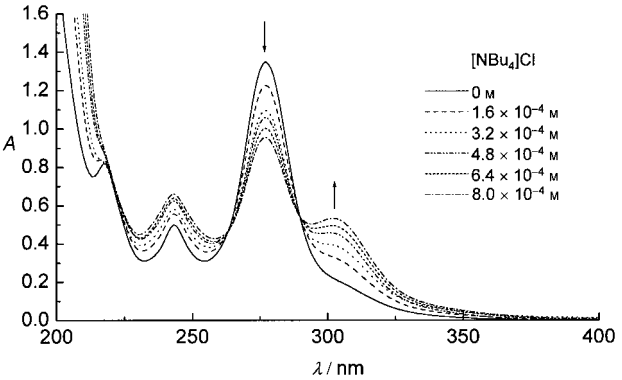

Figure 7. UV/Vis spectral changes of $[Au_2(dcpm)_2]Cl_2$ (**5**) in degassed acetonitrile at room temperature as a function of the $[NBu_4]Cl$ concentration.

$$[Au_2(dcpm)_2]^{2+} + X^- \rightleftharpoons [Au_2(dcpm)_2]X^+ \quad (2)$$

We also note that there is a red-shift in the absorption maxima of $[Au_2(dcpm)_2]X^+$ as X^- changes from Cl^- to Br^- and I^- ($\lambda_{max} = 302$ (Cl^-), 310 (Br^-) and 323 (I^-) nm). However, the extent of the red-shift is smaller than the related changes in LMCT $[p\pi(X^-) \rightarrow Pt(\pi)]$ energies of $[Pt_2(P_2O_5H_2)_4X_2]^{4-}$ ($X^- = Cl^-$, Br^-, I^-, NO_2^-, SCN^-).[1b, 14] We suggest that the electronic transitions of $[Au_2(dcpm)_2]X^+$ at $\lambda = 302$–323 nm are $d\sigma^*(Au) \rightarrow p\sigma(Au)$ in origin. Interactions between the $d_{z^2}(Au)$ and $p\sigma(Au{-}X)$ orbitals account for the small red-shift in the absorption maxima from Cl^- to Br^- and I^-. Equilibrium constants (K) for the reaction given in Equation (2) can be calculated according to Equation (3):[13]

$$K = \frac{x}{([Au_2^{2+}]_0 - x)([X^-]_0 - x)} \quad (3a)$$

$$x = \frac{A - \varepsilon_{Au_2^{2+}}[Au_2^{2+}]_0}{\varepsilon_{Au_2X^+} - \varepsilon_{Au_2^{2+}}} \quad (3b)$$

in which x is the concentration of $[Au_2(dcpm)_2]X^+$; A is the absorbance at the observed wavelength; $[Au_2^{2+}]_0$ and $[X^-]_0$ are the initial concentrations of $[Au_2(dcpm)_2](SO_3CF_3)_2$ and $[NBu_4]X$, respectively, and ε is the extinction coefficient in $mol^{-1}\,dm^3\,cm^{-1}$ of the species designated by the subscript. The simulated UV/Vis spectral changes show good agreement with the experimental data, and the simulated association constants for $[Au_2(dcpm)_2]^{2+}$ with Cl^-, Br^- and I^- in acetonitrile are $(1.8 \pm 0.7) \times 10^3$, $(5.1 \pm 1.0) \times 10^3$ and $(43 \pm 21) \times 10^3\,M^{-1}$, respectively (see the Experimental Section). These values are smaller than those values of 10^4–10^5 for $[Au_2(dmpm)_2]^{2+}$ or $[Au_2(dmpe)_2]^{2+}$ complexes;[13] this can be attributed to the bulkiness of the cyclohexyl substituents.

Solid-state emission: Upon excitation at $\lambda = 280$ nm, complexes **1**–**4** exhibit intense photoluminescence with λ_{max} at 368 nm in the solid state at room temperature (Figure 8). The

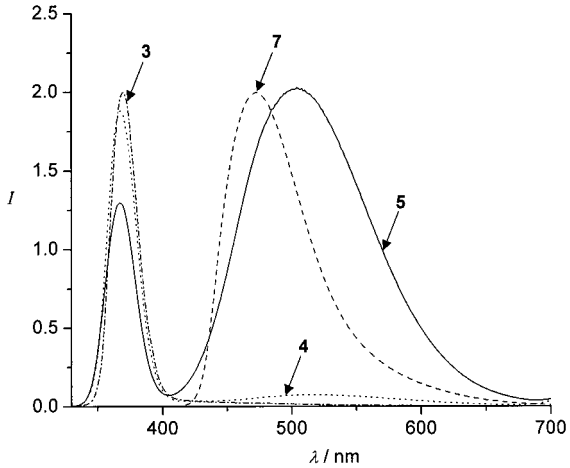

Figure 8. Room-temperature solid-state emission spectra of $[Au_2(dcpm)_2](SO_3CF_3)_2$ (**3**), $[Au_2(dcpm)_2][Au(CN)_2]_2$ (**4**), $[Au_2(dcpm)_2]Cl_2$ (**5**) and $[Au_2(dcpm)_2]I_2$ (**7**) with excitation at $\lambda = 280$ nm. I = intensity.

measured emission quantum yields of powdered samples were 0.37 (**1**), 0.74 (**2**), 0.53 (**3**) and 0.12 (**4**). The high solid-state emission quantum yields reflect the fact that the $[Au_2(dcpm)_2]Y_2$ solids are highly luminous materials in the near UV-region.[15] Solids **1** and **2** also display weak visible emissions at $\lambda = 564$ and 505 nm, respectively, but this type of emission was not found for **3**. For solid **4**, the visible emission at $\lambda = 515$ nm was found to be more intense than that of solids **1** and **2**. Both the high- (360–370 nm) and low-energy (500–570 nm) emissions have lifetimes on the microsecond timescale; this implies that these emissions are from the triplet-parentage excited states. As discussed in a previous communication,[2b] the high-energy emission is ascribed to intrinsic phosphorescence from the $^3[d\sigma^*p\sigma]$ excited state. With this assignment, the Stokes shift in energy between the $^1[d\sigma^*p\sigma]$ absorption and $^3[d\sigma^*p\sigma]$ emission for the $[Au_2(dcpm)_2]^{2+}$ complex is 8930 cm^{-1}, which compares well with 7793 cm^{-1} found for the $[Pt_2(P_2O_5H_2)_4]^{4-}$ system.[1b] The 277 nm absorption and the 368 nm emission bands have a similar band-shape, which serves as evidence of common/similar electronic origin(s).

For complexes **6** and **7**, only the visible emissions are observed from their solid samples at room temperature (Figure 8). Emission quantum yields of powdered samples upon excitation at $\lambda = 280$ nm are 0.09 (**6**) and 0.17 (**7**). These quantum yields are significantly lower than those of the high-energy UV ones for complexes **1**–**3**. The crystalline solid $[Au_2(dcpm)_2](SCN)_2$ (**6**) shows only one intense emission band with λ_{max} at 465 nm at room temperature. The two isolated crystalline forms of **7a** and **7b** display different emission energies. The room-temperature solid-state emission maxima for $[Au_2(dcpm)_2]I_2$ and $[Au_2(dcpm)_2]I_2 \cdot 0.5\,CH_2Cl_2$ are 473 and 486 nm, respectively. It is particularly interesting that the two compounds have virtually the same bonding parameters. The inclusion of CH_2Cl_2 molecules into the crystal lattice of $[Au_2(dcpm)_2]I_2$ causes a red-shift in the emission energy.

As stated in a previous section, the UV/Vis absorption spectrum of **7** is different from that of $[Au_2(dcpm)_2]^{2+}$, consistent with complexation between $[Au_2(dcpm)_2]^{2+}$ and I^-. The low-energy solid-state photoluminescence of this complex is, therefore, attributed to the excited state associated with the three-coordinate AuP_2I moiety. For complexes **1**–**3**, the Au···anion contact distances are significantly longer than that of **7**. Therefore, the effect of the neighbouring anion on the $^3[d\sigma^*p\sigma]$ excited state of $[Au_2(dcpm)_2]^{2+}$ is weaker. This accounts for the intense high-energy emission at $\lambda = 368$ nm for the former three complexes. Complex **4** is an intermediate case, since the Au···anion contact distance lies between that of **1** or **2** and **7**. We found that the visible emission of **4** is more intense than that of **1** and **2**, but is not as intense as the 473 nm emission of solid **7a**.

Complex **5** displays both high- and low-energy emissions with λ_{max} at 366 and 505 nm, respectively (Figure 8). The overall solid-state emission quantum yield is 0.23. The X-ray crystal structure of this complex shows a close Au···Cl contact for one of the two gold atoms. The change in the relative intensities between the high-energy UV and low-energy visible emissions across **1**–**7** (Figure 8 and Table 1 of Ref. [2b]) is parallel with the variation of the Au···anion interaction. This suggests that the cation···anion interaction, either ionic or covalent, has a significant effect on the photoluminescence of the gold(I) solids.

Solution emission: In acetonitrile, all the complexes show emission with λ_{max} ranging from 490 to 530 nm (Figure 9). The high-energy emission at 368 nm is extremely weak. In dichloromethane, there is no detectable emission. The excitation spectra of the visible emissions obtained with dilute acetonitrile solutions are identical to their absorption spectra (Figure 9).

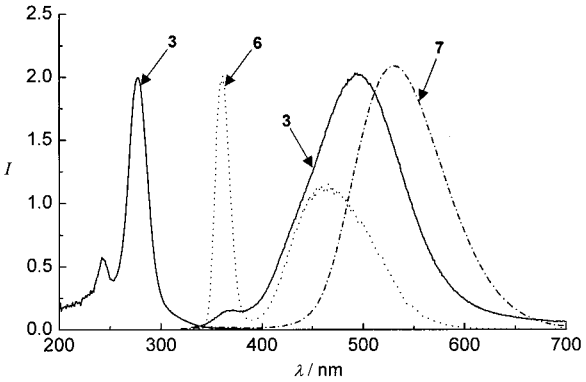

Figure 9. Excitation (left, emission monitored at $\lambda = 500$ nm) and emission (right) spectra of $[Au_2(dcpm)_2](SO_3CF_3)_2$ (**3**), emission spectrum of $[Au_2(dcpm)_2]I_2$ (**7**) with excitation at $\lambda = 280$ nm in degassed acetonitrile at room temperature, and emission spectrum of $[Au_2(dcpm)_2](SCN)_2$ (**6**) with excitation at $\lambda = 280$ nm in EtOH/MeOH (1:4 v/v) at 77 K. I = intensity.

We have also studied the effect of halide ion concentration on the emission. Initial addition of a small amount of $[NBu_4]X$ to $[Au_2(dcpm)_2](SO_3CF_3)_2$ in acetonitrile led to an enhancement of the emission intensity and red-shift in the emission maxima from 508 to 510 (Cl^-), 514 (Br^-) and 530 nm (I^-). Further addition of $[NBu_4]X$ resulted in a decrease of the emission intensity.

In EtOH/MeOH (1:4 v/v) glassy solutions at 77 K, the gold(I) complexes, with the exception of **7**, display a high-energy emission at $\lambda \approx 368$ nm (Figure 9). Complex **7** shows a low-energy emission with λ_{max} at 460 nm. It should be noted that their solid-state emission spectra are similar. A weak emission at $\lambda = 420$–490 nm was observed for complexes **1**–**6** (Table 1 in Ref. [2b]).

Emission quenching and time-resolved absorption studies: Addition of $[NBu_4]X$ ($X = ClO_4^-$, PF_6^-, Cl^- and I^-) quenched the emission of $[Au_2(dcpm)_2]X_2$ in acetonitrile, as illustrated by the plots shown in Figure 10. The observed decrease in emission intensity with $[X^-]$ follows the Stern–Volmer equation [Eq. (4)]:

$$\iota_0/\iota = 1 + k_q\iota_0[X] \qquad (4)$$

in which ι_0 and ι are the luminescent lifetimes in the absence and presence of X^-, and k_q is the quenching rate constant. The k_q values are 6.08×10^5, 9.18×10^5, 1.55×10^7 and 4.06×10^9 $mol^{-1}\,dm^3\,s^{-1}$ for ClO_4^-, PF_6^-, Cl^- and I^-, respectively. The quenching rate constant for the I^- ion is particularly

0947-6539/01/0721-4660 $ 17.50+.50/0 *Chem. Eur. J.* **2001**, *7*, No. 21

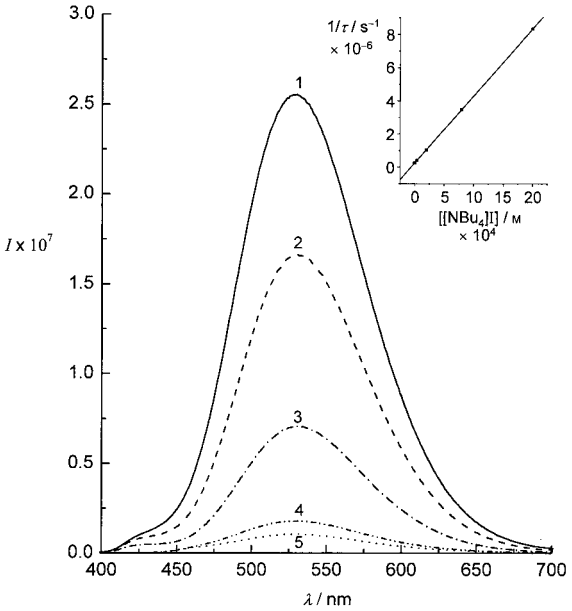

Figure 10. Room-temperature emission spectra of $[Au_2(dcpm)_2]I_2$ (**7**) in the presence of varying concentrations of $[NBu_4]I$ in degassed acetonitrile with excitation at $\lambda = 280$ nm. Concentration of $[NBu_4]I$: 1) 0 M, 2) 4×10^{-5} M, 3) 2×10^{-4} M, 4) 8×10^{-4} M, 5) 2×10^{-3} M. I = intensity.

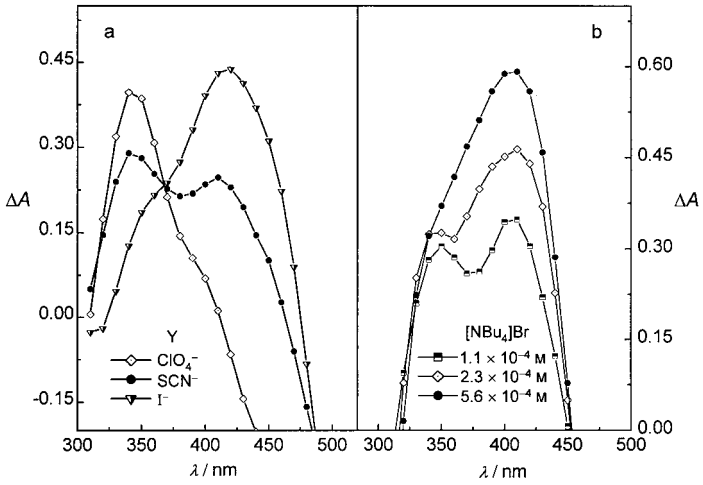

Figure 11. a) Room-temperature transient difference-absorption spectra of $[Au_2(dcpm)_2]Y_2$ (Y = ClO_4^-, SCN^-, I^-) monitored after 1.5 μs pulsed excitation at $\lambda = 266$ nm in degassed acetonitrile solution. b) Room-temperature transient difference-absorption spectra of $[Au_2(dcpm)_2](SO_3CF_3)_2$ (**3**) (5.1×10^{-5} M) in various $[NBu_4]Br$ concentrations monitored after 1.5 μs pulsed excitation at $\lambda = 266$ nm in degassed acetonitrile solution.

large: it is 10^3 times larger than those with the ClO_4^- or PF_6^- ions. To probe the quenching mechanism, we have studied the effect of the counterion on the triplet-state difference absorption spectra of $[Au_2(dcpm)_2]^{2+}$.

The triplet-state difference absorption spectra of solutions of $[Au_2(dcpm)_2]Y_2$ in acetonitrile were measured after nanosecond-pulsed excitation at $\lambda = 266$ nm. Assignment of the difference absorption spectra to the triplet excited state is confirmed by the excellent match of the decay lifetime of the absorption signal with that of the emission. In the absence of any added counterion, the spectra for complexes **1**–**4**, recorded 1.5 μs after excitation, are similar and characterised by an absorption maxima at $\lambda = 350$ nm with a shoulder at ≈ 395 nm. The 350 nm absorption, with a decay rate constant comparable to the emission lifetime, is assigned to the triplet excited state of $[Au_2(dcpm)_2]^{2+}$, while the 395 nm shoulder, with a much longer decay lifetime, is attributed to $[Au_2X^+/Au_2S^{2+}]^*$ via $X^-/S + Au_2^{2+*} \rightarrow [Au_2X^+/Au_2S^{2+}]^*$ states. With this assignment, the absorbance of Au_2X^{+*} is affected by X^-. The transient absorption spectra for the complexes $[Au_2(dcpm)_2]Y_2$ were measured as a function of the halide concentration. The results are presented in Figures 11–13. As the anion is changed from ClO_4^- to SCN^- and I^- (Figure 11a), the absorption maxima at 350 nm decreases in intensity; however, there is a concomitant development of a lower energy absorption at 420 nm, the decay lifetime of which is much longer than the decay lifetime measured at 350 nm. Typical spectral changes observed for complex **5** with different Cl^- concentrations are shown in Figure 12. There is a shift in the absorption maxima from $\lambda = 350$ to ≈ 410 nm with increasing Cl^- concentrations. Therefore, the equilibrium given in Equation (5) is suggested to occur.

$$[Au_2(dcpm)_2^{2+}]^* + Cl^- \rightleftharpoons [Au_2(dcpm)_2Cl^+]^* \quad (5)$$
$$\text{350 nm} \qquad\qquad \text{410 nm}$$

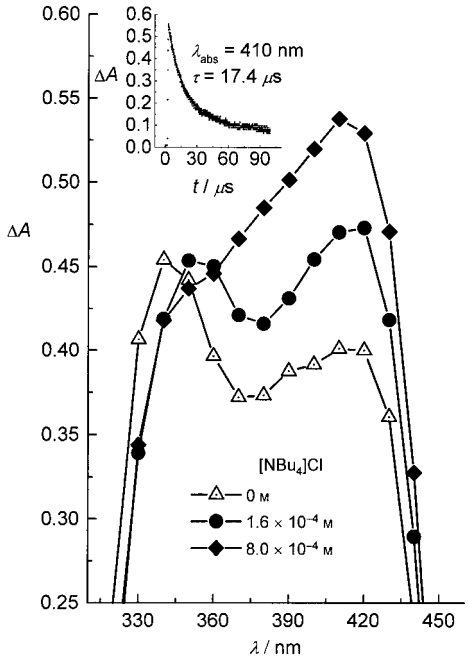

Figure 12. Room-temperature transient difference-absorption spectra of $[Au_2(dcpm)_2]Cl_2$ (**5**) (7.5×10^{-5} M) in various $[NBu_4]Cl$ concentrations monitored after 1.5 μs pulsed excitation at $\lambda = 266$ nm in degassed acetonitrile solution. Inset: decay traces of transient difference-absorption spectra of $[Au_2(dcpm)_2]Cl_2$ (**5**) (7.5×10^{-5} M) in $[NBu_4]Cl$ (8.0×10^{-4} M) monitored at $\lambda = 410$ nm.

It should be noted that the decay lifetime measured at $\lambda = 410$ nm (ι, 17.4 μs) is substantial. Similar results have been obtained with solutions of complex **3** in acetonitrile in the presence of varying concentrations of $[NBu_4]Br$ (Figure 11b).

As shown in Figure 11a, the triplet-state difference absorption spectrum for complex **7** shows an intense absorption peak at $\lambda = 420$ nm and a shoulder at ≈ 350 nm; in addition, a weak

absorption at 730 nm is observed. When $[NBu_4]I$ was added to the solution, the 420 nm absorption peak underwent a blue-shift to $\lambda = 400$ nm and the signal intensities at 400 and 730 nm were enhanced with diminution of the 350 nm shoulder (Figure 13). With reference to the previous work by Grossweiner and Matheson,[16–18] the 730 nm absorption maxima can be assigned to the absorption of I_2^-.

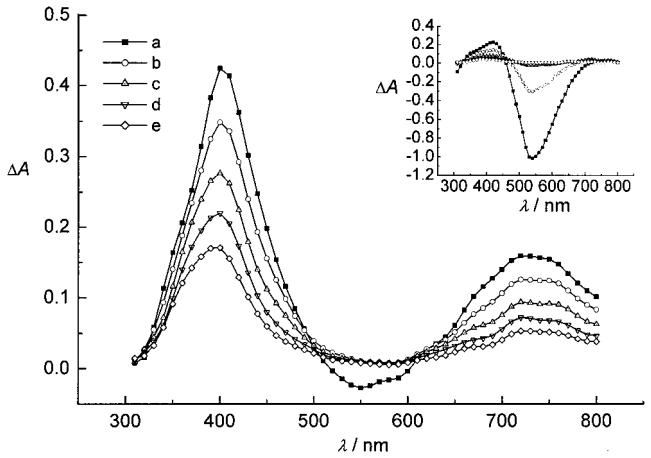

Figure 13. Transient differential absorption spectra of $[Au_2(dcpm)_2]I_2$ (**7**) (4.1×10^{-5} M) in degassed acetonitrile containing $[NBu_4]I$ (8.3×10^{-4} M) after a) 1.2 μs, b) 3.7 μs, c) 8.2 μs, d) 16.5 μs and e) 33.9 μs pulsed excitation at $\lambda = 266$ nm. Inset: $[NBu_4]I$ (5.5×10^{-5} M).

Lifetime measurements showed that there are two decay processes (lifetime = 3.8 and ≈42 μs) for the 400 nm absorption in the triplet-state difference absorption spectrum of **7**. The latter component becomes the major signal at higher $[NBu_4]I$ concentrations. It is assigned to I_2^-. The minor, short-lived component at 400 nm is attributed to the triplet excited state of $[Au_2(dcpm)_2]^+$. We conclude that photolysis of a solution of **7** in degassed acetonitrile results in a photoredox reaction [Eq. (6)].

$$[Au_2(dcpm)_2]^{2+*} + 2I^- \longrightarrow [Au_2(dcpm)_2]^+ + I_2^- \quad (6)$$

Conclusions

It is important to study the factors affecting the photophysical and photochemical properties of luminescent gold(I) complexes, which have been receiving growing interest in the past several years. The open coordination framework of two-coordinate gold(I) is important for it to be able to undergo substrate-binding reactions in the ground and excited states. In this work, high association constants (1.8 to 43×10^3 M^{-1}) of $[Au_2(dcpm)_2]^{2+}$ with halide ions were also determined. The high affinity of two-coordinate gold(I) to undergo substrate-binding reactions is in contrast to the square-planar d^8 platinum(II) system, which remains four-coordinate in most instances. It is of interest to compare the $[Au_2(dcpm)_2]^{2+}$ (Au_2) with the classic dinuclear platinum(II) photocatalyst $[Pt_2(P_2O_5H_2)_4]^{4-}$ (Pt_2). Both the Au_2 and Pt_2 systems have vacant coordination sites at the metal atom, feature an intense $nd\sigma^* \rightarrow (n+1)p\sigma$ transition and have long-lived and emissive $^3[d\sigma^*p\sigma]$ excited states in fluid solutions at room temperature. Importantly, the $[d\sigma^*p\sigma]$ triplet excited states of both systems have a formal metal–metal single bond and are powerful photoreductants. Because $[Pt_2(P_2O_5H_2)_4]^{4-}$ is an effective photocatalyst for C–X bond activation via the reactive $[Pt_2\cdots X{-}C]^*$ intermediate,[1] we envisioned that $[Au_2(diphosphine)_2]^{2+}$ photocatalysts may display similar photochemical reactivities.

However, the $[Au_2(diphosphine)_2]^{2+}$ systems do not react with C–H bonds (including activated ones) photochemically. Even though the $[Au_2(dppm)_2]^{2+}$ (dppm = bis(diphenylphosphino)methane) was reported to catalyze the photochemical cleavage of C–X (X = halide) bonds, the photochemical reaction was found to take place following an electron-transfer mechanism rather than an atom-transfer mechanism.[7] Such a discrepancy in the photochemical properties between the Au_2 and Pt_2 systems was difficult to rationalize prior to this work, given the similar properties of the $^3[d\sigma^*p\sigma]$ excited states of both systems and that both Au^I and Pt^{II} are coordinatively unsaturated. We propose that the apparent lack of reactivity towards C–H bond activation of the triplet excited states of $[Au_2(diphosphine)_2]^{2+}$ is attributed to the fact that the $^3[d\sigma^*p\sigma]$ state of Au_2 exists as a solvent/anion exciplex in solution, rendering the gold(I) less accessible towards interacting with the C–H bond by an inner-sphere pathway. Indeed the high affinity of the $^3[d\sigma^*p\sigma]$ excited state of $[Au_2(diphosphine)_2]^{2+}$ toward substrate-binding reactions has also been confirmed by molecular orbital calculations, as described in previous works.[19]

We propose that the high-energy $^3[d\sigma^*p\sigma]$ emission should be present for any $[Au_2(diphosphinomethane)_2]Y_2$ compound in which Y is a non-coordinating anion. The fact that $[Au_2(dppm)_2](ClO_4)_2$ shows no intense high-energy emission in the solid state at room temperature deserves attention.[7a, 9a] The only difference between $[Au_2(dppm)_2](ClO_4)_2$ and **1** is the auxiliary phosphine ligand, namely phenyl- versus cyclohexyl-substituted diphosphines. The phenyl rings of the dppm ligand have their $^3(\pi\pi^*)$ state [the $^3(\pi\pi^*)$ emission of $[Cy_3PAu\text{-}Ph]$ is at ≈347 nm in CH_3CN] close in energy to the intrinsic $^3[d\sigma^*p\sigma]$ emission of $[Au_2(dppm)_2]^{2+}$; there may be a deactivating state for the latter through an intramolecular energy-transfer process. The neighbouring counteranion is an important factor affecting the high-energy emission of the $[Au_2(diphosphinomethane)_2]Y_2$ solid. For soft anions, such as I^-, clear evidence exists for the complexation of the ground state, and Au-anion complexation in the excited state would quench the $^3[d\sigma^*p\sigma]$ high-energy emission. It is no wonder that only low-energy emission attributed to three-coordinate gold(I) species can be observed in the solid-state emission spectra of **6** and **7** at room temperature, but not for the other gold complexes.

Experimental Section

Materials: The salt $K[AuCl_4]$ (Johnson Matthey Chemicals), thiodiglycol (2,2′-thiodiethanol, Aldrich) and dcpm (Strem) were used as received. $[Au_2(dcpm)_2]Y_2$ ($Y = ClO_4^-, PF_6^-, SO_3CF_3^-$) complexes were prepared in a

0947-6539/01/0721-4662 $ 17.50+.50/0 *Chem. Eur. J.* **2001**, *7*, No. 21

similar manner to $[Au_2(dppm)_2](ClO_4)_2$.[7] Solvents (spectroscopic grade) used in the spectroscopic studies were dried over suitable reagents and distilled under an argon atmosphere prior to use.

$[Au_2(dcpm)_2]Y_2$ (Y = ClO_4^- (1), PF_6^- (2), $SO_3CF_3^-$ (3), Cl^- (5)): Thiodiglycol (0.22 mL, 2.12 mmol) was added to a stirred solution of $K[AuCl_4]$ (0.4 g, 1.06 mmol) in methanol (40 mL), followed by addition of solid dcpm (0.4 g, 1.04 mmol). A pale yellow solid precipitated, which dissolved upon warming to give a colourless solution that was filtered. Addition of excess $LiClO_4$, NH_4PF_6 or $NH_4SO_3CF_3$ to the filtrate produced white precipitates, which were collected by filtration, and washed with distilled water and diethyl ether. To purify the solids they were recrystallised from acetonitrile by slow evaporation. Compound **5** was obtained as crystals by diffusion with diethyl ether. The compounds were characterised by ^{31}P NMR spectroscopy and X-ray crystallography. ^{31}P NMR (acetonitrile): $\delta = 54.1$ for **1**–**3**; 52.9 for **5**.

$[Au_2(dcpm)_2][Au(CN)_2]_2$ (4): Solid dcpm (0.2 g, 0.52 mmol) was added to a solution of $K[AuCl_4]$ and thiodiglycol in methanol as described above. The solid $[Au_2(dcpm)]Cl_2$ was obtained after removal of the solvent. NaCN (0.0225 g, 0.46 mmol) was then added to a solution of $[Au_2(dcpm)]Cl_2$ (0.2 g, 0.23 mmol) in dichloromethane (20 mL). After stirring for 2 h, the mixture was filtered and the filtrate was concentrated to ≈4 mL by rotary evaporation. Slow addition of hexane afforded a white precipitate, which was collected by filtration, washed with distilled water and hexane, and recrystallised from acetonitrile/dichloromethane. The crystalline solid was characterised by ^{31}P NMR and X-ray crystallography. ^{31}P NMR (acetonitrile): $\delta = 54.1$.

$[Au_2(dcpm)_2]Y_2$ (Y = SCN^- (6) and I^- (7)): Compounds **6** and **7** were prepared in a similar manner to **1**. Addition of excess NaI to a solution of $K[AuCl_4]$, thiodiglycol and dcpm in methanol afforded a yellowish powder. Recrystallisation by slow evaporation from an acetonitrile or dichloromethane solution produced two different crystalline solids: one was white while the other was greenish-yellow. The two crystalline solids were characterised by ^{31}P NMR and X-ray crystallography. ^{31}P NMR (acetonitrile): $\delta = 48.5$ for both crystals ($[Au_2(dcpm)_2]I_2$ and $[Au_2(dcpm)_2]I_2 \cdot 0.5\,CH_2Cl_2$). When NaSCN was used as a precipitant, a crystalline solid was obtained and characterised by ^{31}P NMR and X-ray crystallography. ^{31}P NMR (acetonitrile): $\delta = 50.1$.

Equipment and procedures: Steady-state absorption spectra were recorded at ambient temperature with a HP8453 UV-Vis spectrophotometer. Crystals of suitable size were mounted either on glass fibres or in capillary tubes. X-ray data were collected on either an MAR PSD diffractometer or a Rigaku AFC7R diffractometer. Intensity data were collected by $\omega - 2\theta$ scans. The images were interpreted and integrated by means of the DENZO or ABSOR software. The structures were solved by direct methods (SIR 92) or the Patterson method (PATTY) and expanded by the Fourier method. Structural refinement on F or F^2 by full-matrix least-square analysis was performed with the TeXsan, SHELXL-93 or NRCC-SDP VAX programs. ORTEP drawings of the structures are displayed with hydrogen atoms omitted for clarity.

Crystallographic data for the structures reported in this paper have been deposited with the Cambridge Crystallographic Data Centre as supplementary publication nos. CCDC-116329 (**1**), CCDC-116330 (**4**), CCDC-116331 (**7a**), CCDC-150222 (**5**), CCDC-158872 (**6**), CCDC-158873 (**7b**). Copies of the data can be obtained free of charge on application to CCDC, 12 Union Road, Cambridge CB21 EZ, UK (fax: (+44) 1223-336-033; e-mail: deposit@ccdc.cam.ac.uk).

The equilibrium constants for the complexation of $[Au_2(dcpm)_2]^{2+}$ with halides were simulated by Marquardt fits. All the simulation calculations were performed by SPECFIT packages. The raw experimental data in ASCII format was edited by a text editor to make them compatible with the input format of SPECFIT before they were read by the program.

Corrected emission and excitation spectra were obtained on a SPEX Fluorolog-2 Model F111A1 fluorescence spectrofluorometer adapted to a right-angle configuration. Filters of suitable bandpass were used to cut off the second harmonic of the monochromatic excitation light source and stray light. Solutions for excitation or emission measurements were degassed by at least four freeze-pump-thaw cycles. Low-temperature (77 K) emission spectra for glass and solid-state samples were recorded for 5 mm diameter quartz tubes which were placed inside a liquid nitrogen bath placed in a quartz optical Dewar flask.

Measurement of emission quantum yields of powdered samples involved the determination of the diffuse reflectance of the $[Au_2(dcpm)_2]Y_2$ complex relative to KBr at the excitation wavelength.[20] The measured results were corrected according to the relative response of the detector as a function of the wavelength. Emission lifetimes of solid or solution samples were performed with a Quanta Ray DCR-3 Nd-YAG laser with pulse-width of 8 ns and excitation wavelength of 355 nm (third harmonic) or 266 nm (fourth harmonic). Emission signals were collected at right angles to the excitation pulse by a Hamamatsu R928 photomultiplier tube and recorded on a Tektronix model 2430 digital oscilloscope.

Stern–Volmer quenching measurements were carried out with degassed solutions of the metal complex in the presence of a quencher Q. Linear plots of τ_0/τ versus [Q] were obtained from which bimolecular quenching rate constants, k_q, were deduced according to Equation (4).

Transient absorption spectra were recorded after excitation of the sample in degassed acetonitrile with an 8 ns laser pulse at $\lambda = 266$ nm. The monitoring beam was provided by a 300 W continuous-wave xenon lamp that was oriented perpendicular to the direction of the laser pulse. The transient absorption signals at each wavelength were collected with a SpectraPro-275 monochromator operating with 2 mm slits, with the signal fed to a Tektronix TDS 520D oscilloscope. The optical difference spectrum was generated point-by-point by monitoring at individual wavelengths.

Acknowledgements

We thank the University of Hong Kong and the Hong Kong Research Grants Council [HKU 7298/99P] for financial support.

[1] a) D. M. Roundhill, *J. Am. Chem. Soc.* **1985**, *107*, 4354; b) D. M. Roundhill, H. B. Gray, C.-M. Che, *Acc. Chem. Res.* **1989**, *22*, 55; c) D. C. Smith, H. B. Gray, *Coord. Chem. Rev.* **1990**, *100*, 169.

[2] a) W. H. Chan, T. C. W. Mak, C.-M. Che, *J. Chem. Soc. Dalton Trans.* **1998**, 2275; b) W.-F. Fu, K.-C. Chan, V. M. Miskowski, C.-M. Che, *Angew. Chem.* **1999**, *111*, 2953; *Angew. Chem. Int. Ed.* **1999**, *38*, 2783.

[3] a) D. R. McMillin, J. R. Kirchhoff, K. V. Goodwin, *Coord. Chem. Rev.* **1985**, *64*, 83; b) E. M. Stacy, D. R. McMillin, *Inorg. Chem.* **1990**, *29*, 393.

[4] a) H. Kunkely, A. Vogler, *J. Am. Chem. Soc.* **1990**, *112*, 5625; b) K.-T. Wan, C.-M. Che, K.-C. Cho, *J. Chem. Soc. Dalton Trans.* **1991**, 1077; c) C. N. Pettijohn, E. B. Jochnowitz, B. Chuong, J. K. Nagle, A. Vogler, *Coord. Chem. Rev.* **1998**, *171*, 85.

[5] a) K.-S. K. Shin, J. D. Barrie, B. Dunn, J. I. Zink, *J. Am. Chem. Soc.* **1990**, *112*, 5701; b) M. A. Omary, H. H. Patterson, *J. Am. Chem. Soc.* **1998**, *120*, 7696.

[6] N. P. Ayala, C. M. Flynn, Jr., L. Sacksteder, J. N. Demas, B. A. DeGraff, *J. Am. Chem. Soc.* **1990**, *112*, 3837.

[7] a) C.-M. Che, H.-L. Kwong, V. W.-W. Yam, K.-C. Cho, *J. Chem. Soc. Chem. Commun.* **1989**, 885; b) D. Li, C.-M. Che, H.-L. Kwong, V. W.-W. Yam, *J. Chem. Soc. Dalton Trans.* **1992**, 3325.

[8] a) L. H. Gade, *Angew. Chem.* **1997**, *109*, 1219; *Angew. Chem. Int. Ed. Engl.* **1997**, *36*, 1171; b) J. C. Vickery, M. M. Olmstead, E. Y. Fung, A. L. Balch, *Angew. Chem.* **1997**, *109*, 1227; *Angew. Chem. Int. Ed. Engl.* **1997**, *36*, 1179.

[9] a) C. King, J.-C. Wang, M. N. I. Khan, J. P. Fackler, Jr., *Inorg. Chem.* **1989**, *28*, 2145; b) M. N. I. Khan, C. King, D. D. Heinrich, J. P. Fackler, Jr., L. C. Porter, *Inorg. Chem.* **1989**, *28*, 2150; c) Z. Assefa, B. G. McBurnett, R. J. Staples, J. P. Fackler, Jr., B. Assmann, K. Angermaier, H. Schmidbaur, *Inorg. Chem.* **1995**, *34*, 75.

[10] a) S.-J. Shieh, X. Hong, S.-M. Peng, C.-M. Che, *J. Chem. Soc. Dalton Trans.* **1994**, 3067; b) B.-C. Tzeng, W.-C. Lo, C.-M. Che, S.-M. Peng, *Chem. Commun.* **1996**, 181; c) B.-C. Tzeng, C.-M. Che, S.-M. Peng, *Chem. Commun.* **1997**, 1771; d) B.-C. Tzeng, C.-K. Chan, K.-K. Cheung, C.-M. Che, S.-M. Peng, *Chem. Commun.* **1997**, 135.

[11] K. H. Leung, D. L. Phillips, M-C. Tse, C.-M. Che, V. M. Miskowski, *J. Am. Chem. Soc.* **1999**, *121*, 4799.

[12] H. Schmidbaur, *Chem. Soc. Rev.* **1995**, *24*, 391.

[13] H. R. C. Jaw, M. M. Savas, R. D. Rogers, W. R. Mason, *Inorg. Chem.* **1989**, *28*, 1028.

[14] C.-M. Che, L. G. Butler, P. J. Grunthaner, H. B. Gray, *Inorg. Chem.* **1985**, *24*, 4662.
[15] Y. Ma, C.-M. Che, H.-Y. Chao, X. Zhou, W.-H. Chan, J. Shen, *Adv. Mater.* **1999**, *11*, 852.
[16] a) L. I. Grossweiner, M. S. Matheson, *J. Phys. Chem.* **1957**, *61*, 1089; b) M. S. Matheson, W. A. Mulac, J. Rabani, *J. Phys. Chem.* **1963**, *67*, 2613.
[17] a) M. E. Langmuir, E. Hayon, *J. Phys. Chem.* **1967**, *71*, 2613; b) H. D. Burrows, *Inorg. Chem.* **1990**, *29*, 1549.
[18] G. L. Hug, *Optical Spectra of Nonmetallic Inorganic Transient Species in Aqueous Solution*, NSRDS-NBS 69, National Bureau of Standards, Washington DC, **1981**.
[19] H. X. Zhang, C.-M. Che, *Chem. Eur. J.*, in press.
[20] M. S. Wrighton, D. S. Ginley, D. L. Morse, *J. Phys. Chem.* **1974**, *78*, 2229.

Received: April 17, 2001 [F3203]

0947-6539/01/0721-4664 $ 17.50+.50/0